

Optical actinometry of Cl_2 , Cl , Cl^+ , and Ar^+ densities in inductively coupled Cl_2 -Ar plasmas

N. C. M. Fuller and Irving P. Herman^{a)}

Columbia Radiation Laboratory, Department of Applied Physics, Columbia University,
New York, New York 10027

Vincent M. Donnelly

Agere Systems, Murray Hill, New Jersey 07974

(Received 10 April 2001; accepted for publication 10 June 2001)

Optical emission (OE) actinometry has been used to measure the absolute densities of Cl_2 , Cl , Cl^+ , and Ar^+ in a high-density inductively coupled (ICP) Cl_2 -Ar plasma at 18 mTorr as a function of the 13.56 MHz radio frequency (rf) power and Ar fraction. The fractional dissociation of Cl_2 to Cl increases with rf power, with the dissociated fraction increasing from 78% to 96% at 600 W (10.6 W cm^{-2}) as the Ar fraction increases from 1% to 78% due to an increase in electron temperature. Emission from Cl^{+*} and Ar^{+*} originates primarily from electron excitation of Cl^+ and Ar^+ (and not excitation of Cl and Ar), making actinometric determination of Cl^+ and Ar^+ densities feasible. For powers exceeding 600 W, the neutral (Cl_2 and Cl) to ion (Cl^+ and Ar^+) flux ratio is found to be strongly dependent on Ar fraction, decreasing by a factor of ~ 3.0 as the latter is increased from 13% to 78%. This dependence can be attributed mostly to the decrease in Cl density and relatively little to the small decrease in the total positive ion density from 1.8×10^{11} to $1.4 \times 10^{11} \text{ cm}^{-3}$, over the same range. OE spectroscopy is also used to estimate the rate constant for the dissociative excitation of Cl_2 to the $\text{Cl}(4p^2D^0J'=3/2,5/2)$ excited state with emission at 822.2 nm, yielding $\sim 10^{-13} \text{ cm}^3 \text{ s}^{-1}$. © 2001 American Institute of Physics. [DOI: 10.1063/1.1391222]

I. INTRODUCTION

III-V based semiconductors are in increasingly wide use for a variety of optoelectronic and microelectronic applications. Many have direct band gaps of a wide range in energy, making these materials systems, such as InGaAsP/InP and InGaN/AlGaIn, ideal for photonic device applications such as laser diodes, light emitting diodes (LEDs), and detectors.¹⁻³ The AlGaIn/GaN system is suitable for high temperature and power microelectronic devices⁴ and high speed device applications.⁵ The etching of these materials in manufacturing these devices is critical to device performance and reliability. Consequently, there has been considerable research to determine the most suitable gas chemistry for the plasma chemical etching of these materials.

Cl_2 -Ar based plasmas are emerging as one of the plasma chemistries of choice for etching III-V based semiconductors. Ar is introduced into the plasma because in pure Cl_2 plasma etching of In-containing materials in particular, surface halogenation proceeds relatively more rapidly than ion-induced desorption (sputtering) of the adlayer formed, leading to slow etch rates and a rough surface.⁶ Electron cyclotron resonance (ECR), inductively coupled plasma (ICP), and reactive ion etching (RIE) of AlN, GaN, InN, AlP, GaP, and InP in Cl_2 -Ar based plasmas have been reported.⁶⁻¹² In addition, chemically assisted ion beam etching (CAIBE) of the above materials using Cl_2 molecules and

Ar^+ ions has been investigated.^{13,14} Etch rates from ~ 100 to $\sim 2000 \text{ nm/min}$ have been reported for these materials for a variety of plasma conditions, with InP etching having the slowest rates.⁶⁻¹⁴

The overall etch mechanism, rate, selectivity, and etched profile shapes of these materials depend on the relative fluxes of Cl_2 , Cl , Cl_2^+ , Cl^+ , and Ar^+ in the plasma. In etching, the neutral species, Cl_2 and Cl , are predominantly responsible for chlorinating the surface, while the positive ions (Cl_2^+ , Cl^+ , and Ar^+) sputter this chlorinated surface layer and create sites for subsequent chlorination. Consequently, the determination of the neutral and positively charged species densities as a function of radio frequency (rf) power and Ar fraction is essential in understanding and optimizing plasma etching of these III-V compound semiconductors.

There has been little plasma characterization of high-density, low-pressure Cl_2 -Ar discharges. Eddy *et al.* have used a Langmuir probe to measure plasma densities (n_e), plasma potentials (V_p), and electron temperatures (T_e) as a function of power and Ar fraction in a 1 mTorr Cl_2 -Ar ECR discharge.¹⁵ They also reported the optical emission intensities of several species.

In this article, we report measurements of the absolute densities of all dominant neutral and positively charged species (n_{Cl_2} , n_{Cl} , n_{Cl^+} , and n_{Ar^+}) vs rf power and Ar fraction at 18 mTorr in an inductively coupled (ICP) Cl_2 -Ar discharge. Optical emission spectroscopy (OES) at 306.0 and 822.2 nm from Cl_2 and Cl , respectively, rare gas actinometry¹⁶ using 828.0 nm emission from Xe, and mass

^{a)} Author to whom correspondence should be addressed: electronic mail: iph1@columbia.edu

balance were used to determine n_{Cl_2} and n_{Cl} . OES at 482.0 and 480.7 nm from Cl^+ and Ar^+ , respectively, were used in conjunction with 585.2 nm Ne emission actinometry and electron densities measured by microwave interferometry to determine n_{Cl^+} and n_{Ar^+} . Ion densities were measured in the H -mode (bright, inductive mode) but not in the E -mode (dim, capacitive mode). The density of Cl_2^+ was not measured because previous experiments have shown that the Cl_2^+ density is extremely small in the H -mode.^{17,18}

II. EXPERIMENTAL PROCEDURE

The inductively coupled plasma (ICP) reactor used in these experiments has been described previously.¹⁹ It is comprised of a 6 in. stainless steel cube with four side-facing quartz viewports, one of which is used for light collection. Above a top quartz window is the ICP source, consisting of a four-loop, 8.5 cm diameter coil antenna and matching network. rf power is delivered to the network via a 3 kW Plasma-Therm source operating at 13.56 MHz. For “neat” Cl_2 plasmas, the ICP operates in the E -mode for rf powers ≤ 330 W and in the H -mode at higher rf powers. As the Ar fraction in the Cl_2 -Ar mixture increases, the transition between the two modes occurs at decreasing rf powers. A power of 600 W corresponds to an areal power density of 10.6 W cm^{-2} , for the area defined by the antenna, and a volume power density of 0.7 W cm^{-3} , for the volume defined by the antenna and wafer plane.

In all experiments the pressure, p , in the reactor was 18.0 ± 0.5 mTorr. The flow rates for Cl_2 and Ar were 38.0, 0; 32.0, 4.5; 22.0, 14.5; 8.0, 28.4, and 0, 35.0 sccm for Ar fractions corresponding to 1%, 13%, 40%, 78%, and 96%, respectively. A 5% (1.2 sccm) trace rare gas (TRG) equimixture of He/Ne/Ar/Kr/Xe was added to the gas mixture for the actinometry measurements reported here. A similar method was used for the T_e measurements by TRG-OES to be reported elsewhere.²⁰

No rf power was delivered to the 2 in. diameter sample holder which was positioned ~ 7 cm from the top window. A 2 in. Si $\langle 100 \rangle$ wafer (2–5 $\Omega \text{ cm}$, n type P doped) covered with a 100 nm thick layer of SiO_2 was soldered to the sample holder using In foil. Silicon dioxide etching in Cl_2 discharges proceeds very slowly, and without bias delivered to the sample holder etching occurs at a rate $\ll 0.5$ nm/min due to the small sheath potential (~ 10 V). Such slow etching conditions ensure that the plasma remains relatively unperturbed from etch products; therefore, the results of this study can be applied to Cl_2 -Ar plasma etching of Si, III–V compound semiconductors, and other materials.

Line-integrated plasma induced emission from a region across the wafer and ~ 1.5 cm above it was collected through one of the UV grade quartz windows of the reactor. The emission was imaged by two 6 in. focal length convex quartz lenses onto the entrance slit of a 0.64 m monochromator (ISA Inc., Model No. HR-460) equipped with a GaAs photomultiplier tube (PMT) (Hamamatsu, Model No. R636-10). The slit widths were set to 100 μm for these experiments. Optical emission spectra were obtained by scanning across the appropriate wavelengths at rates varying from 0.2

TABLE I. Emission lines used.

Species	Transition	Wavelength (nm)	Energy threshold (eV)
Cl_2	$4s \sigma_g^1 \pi_g \rightarrow 1 \pi_u$	306.0	8.40
Cl	$4p^2 D^0 J' = 5/2 \rightarrow 4s^4 P$	822.2	10.50
Xe	$2p_5 \rightarrow 1s_4$	828.0	9.94
Cl^+	$3p^3 4p^3 F \rightarrow 3d^3 F^0$	482.0	18.20
Ar^+	$3p^4 4p^4 P^0 \rightarrow 4s^4 P$	480.7	19.20
Ne	$2p_1 \rightarrow 1s_2$	585.2	18.90

to 0.5 nm/s, with a 0.175 nm bandpass. The emission intensities were corrected for the spectral properties of the monochromator and PMT.

III. RESULTS

Optical emission intensities were recorded from 270 to 320 nm for Cl_2 , from 475 to 485 nm for Cl^+ and Ar^+ , at 585.2 nm for Ne, and from 745 to 885 nm for Cl, Ar, Kr, and Xe as a function of rf power and Ar fraction. Absolute number densities of Cl_2 and Cl were determined using rare gas actinometry¹⁶ using Xe emission, and absolute Cl^+ and Ar^+ densities were derived using Ne emission actinometry. The wavelengths, assignments, and threshold energies for the relevant emissions are given in Table I.

A. Cl_2 , Cl, and Xe emission and absolute densities of Cl_2 and Cl

The integrated intensities from the Cl_2 emission band centered at 306.0 nm, assigned to the $4s \sigma_g^1 \pi_g \rightarrow 1 \pi_u$ transition, are presented in Fig. 1, along with integrated emission intensities of Cl at 822.2 nm, corresponding to the $4p^2 D^0 J' = 5/2 \rightarrow 4s^4 P$ transition. Also included in Fig. 1 is the integrated emission intensity from the $2p_5$ Paschen level of Xe at 828.0 nm. Figure 1 spans the lowest E -mode to highest H -mode powers investigated. The abrupt discontinuity in emission intensities at ~ 350 W is a clear indication of the transition between the power-coupling modes.

Emission from Xe ($2p_5$) is excited predominantly by electron impact excitation from the ground state and, to a lesser degree, electron impact excitation from the $1s_3$ and $1s_5$ metastable states.^{21,22} In the E -mode, ground state excitation is responsible for $\sim 95\%$ of the Xe 828.0 nm emission, while in the H -mode it is responsible for only $\sim 70\%$ of the emission, with metastable excitation contributing the rest.

The Cl_2 to Xe number density ratio in the plasma is related to the Cl_2 -to-Xe emission (I) ratio by²²

$$\frac{n_{\text{Cl}_2}}{n_{\text{Xe}}} = a'_{\text{Xe}}(T_e, n_e, l, p) b_{\text{Cl}_2, \text{Xe}} \frac{I(\text{Cl}_2, 306.0)}{I(\text{Xe}, 828.0)}. \quad (1)$$

The factor $a'_{\text{Xe}}(T_e, n_e, l, p)$, where l is the effective reactor length, accounts for the contribution of metastables and it is computed from a model described elsewhere.²² It is 1.05 (1/0.95) in the E -mode and 1.4 (1/0.7) in the H -mode. The constant $b_{\text{Cl}_2, \text{Xe}}$ is the ratio of the excitation rate of Xe^* to that of Cl_2^* . In principle it could be computed from Cl_2 and

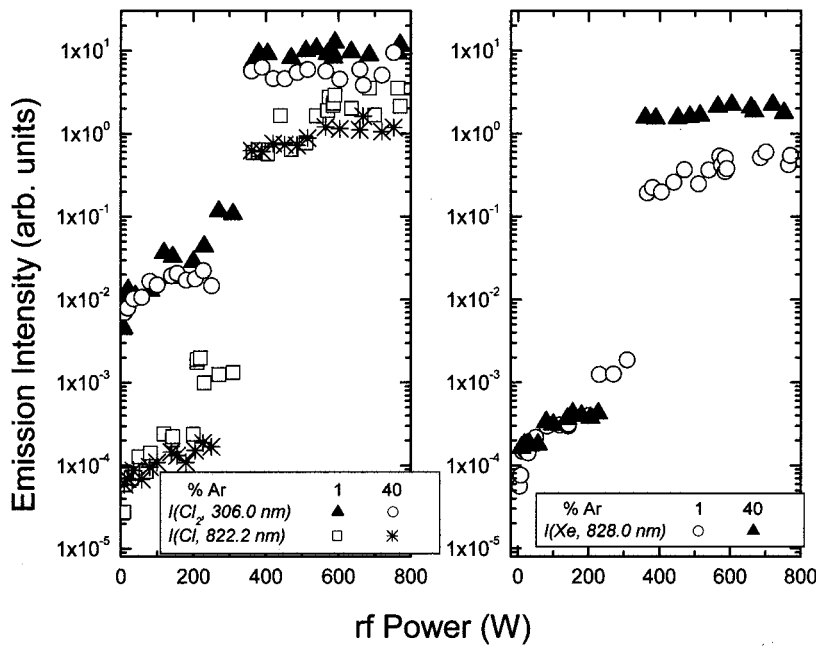


FIG. 1. Optical emission intensity vs rf power for the Cl_2 emission band centered at 306.0 nm, the Cl emission line at 822.2 nm, and the Xe emission line at 828.0 nm in an 18 mTorr Cl_2 -Ar ICP plasma with 5% of the trace rare gas mixture. Data are shown here only for the mixtures with 1% and 40% Ar. All data have been corrected for the wavelength-dependent response of the spectrometer and photomultiplier tube.

Xe electron impact cross sections. While the Xe cross section has been reported, the Cl_2 cross section has not. Consequently, $b_{\text{Cl}_2,\text{Xe}}$ must be measured. This is easily done by extrapolating the Cl_2 to Xe emission ratio to the limit of zero rf power, where n_{Cl_2} approaches the initial Cl_2 gas density before the plasma is ignited.²²

The electron energy thresholds for electron impact excitation of ground state Cl_2 and Xe to their excited states of interest here are 8.40 and 9.94 eV, respectively. Despite this 1.54 eV energy difference, $b_{\text{Cl}_2,\text{Xe}}$ has been found to be relatively independent of T_e . Nonetheless, $b_{\text{Cl}_2,\text{Xe}}$ was determined for each Ar fraction. Within experimental error, $b_{\text{Cl}_2,\text{Xe}}$, corrected for gas transport²² (see below) was independent of the Cl_2 to Ar flow rate ratio. When the integrated Cl_2 intensities were divided by the Cl_2 bandwidth, to make $b_{\text{Cl}_2,\text{Xe}}$ directly comparable with those in a previous study and independent of spectrometer resolution, they ranged from 460 to 696 with an average value of 596, in excellent agreement with the reported value of 555.²²

To obtain absolute Cl_2 number densities, the reduction in the total number density due to heating of the gas must be taken into account. Since the plasma volume (V_p) is about equal to the cold, dead volume (V_d) that is below the plasma and above the first flow-restricting element in the pumping line (a 2.0 cm diameter aperture), a simple inverse temperature scaling of gas number density for uniform pressure conditions does not apply. For a mean free path for neutrals (~ 3 mm) much smaller than the effective chamber length, the change in neutral number density can be estimated using

$$\delta(T_g, T_w) = \frac{(V_p/V_d) + 1}{(V_p/V_d) + (T_g/T_w)}, \quad (2)$$

to obtain the number density of an inert gas (e.g., Xe)²²

$$n_{\text{Xe}} = n_{\text{Xe}}^0 \delta(T_g, T_w), \quad (3)$$

where n_{Xe}^0 and T_w ($=300$ K) are the Xe number density and gas temperature with the plasma off (=the wall temperature), and T_g is the gas temperature when the plasma is on. The gas temperature was not measured in these experiments, but, based on prior measurements of gas temperatures in Cl_2 ICPs,^{23,24} was assumed to vary linearly from the wall temperature (300 K) at 350 W to ~ 1200 K at 800 W for all Ar fractions. The final expression for Cl_2 number density is therefore²²

$$n_{\text{Cl}_2} = a'_{\text{Xe}}(T_e, n_e, l, p) b_{\text{Cl}_2,\text{Xe}} n_{\text{Xe}}^0 \delta(T_g, T_w) \frac{I(\text{Cl}_2, 306.0)}{I(\text{Xe}, 828.0)}. \quad (4)$$

The dependence of n_{Cl_2} on rf power and Ar fraction can now be determined from the emission data shown in Fig. 1 and Eq. (4). These molecular chlorine densities are presented in Fig. 2.

A similar expression can be obtained for Cl number densities in terms of the Cl 822.2 nm to Xe 828.0 nm emission intensity ratios:²²

$$n_{\text{Cl}} = b_{\text{Cl,Xe}} \left[a'_{\text{Xe}}(T_e, n_e, l, p) n_{\text{Xe}}^0 \delta(T_g, T_w) \frac{I(\text{Cl}, 822.0)}{I(\text{Xe}, 828.0)} - \frac{n_{\text{Cl}_2}}{b_{\text{Cl}_2 \rightarrow \text{Cl,Xe}}} \right], \quad (5)$$

where the constants $b_{\text{Cl,Xe}}$ and $b_{\text{Cl}_2 \rightarrow \text{Cl,Xe}}$ in Eq. (5) are the ratios of the rate of exciting Xe^* to that of forming Cl^* by the respectively pathways:



The Cl_2 densities shown in Fig. 2 indicate that Cl_2 dissociation is high in the H-mode; therefore $n_{\text{Cl}} \gg n_{\text{Cl}_2}$ and reaction (7) contributes negligibly to the population of Cl^* .

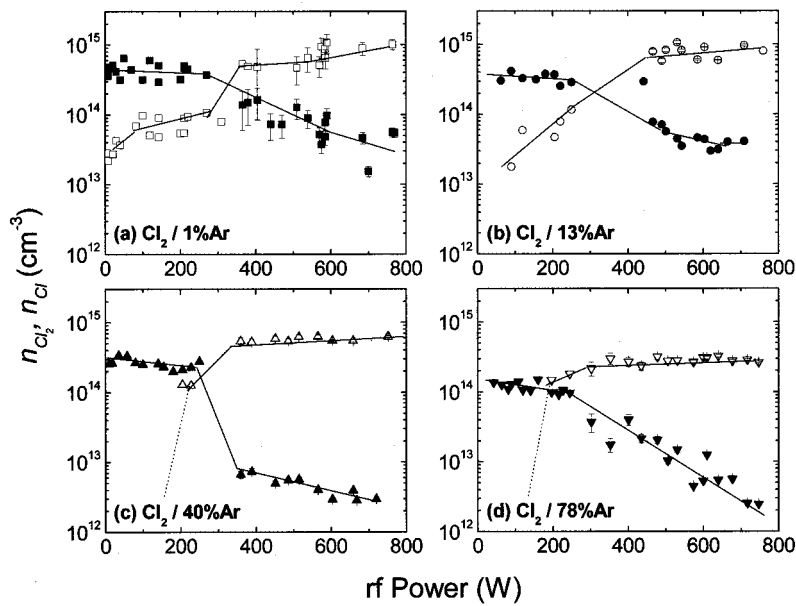


FIG. 2. Absolute densities of Cl (open symbols) and Cl₂ (solid symbols) vs rf power and Ar fraction (1%, 13%, 40%, and 78%) in an 18 mTorr Cl₂-Ar ICP plasma with 5% of the trace rare gas mixture.

Consequently, only the constant $b_{Cl,Xe}$ is needed and it is determined from the Cl atom density calculated using the measured n_{Cl_2} at conditions of very high dissociation and mass balance (it is called n_{Cl}^{calc}) and using the emission ratio $I(Cl,822.2)/I(Xe,828.0)$. From chlorine mass balance:²²

$$n_{Cl}^{calc} = 2[n_{Cl_2}^0 \delta(T_g, T_w) - n_{Cl_2}] S_{eff}(Cl_2) / S_{eff}(Cl), \quad (8)$$

where $n_{Cl_2}^0$ is the initial Cl₂ gas density before the plasma is ignited ($=5.43 \times 10^{14} \text{ cm}^{-3}$ for 1% Ar Cl₂-Ar discharge) and $S_{eff}(A)$ is the effective pumping speed of species A; this enables the computation of the values of $b_{Cl,Xe}$ as a function of the Cl₂-to-Ar feed gas ratio (average value of 52). This procedure is followed for each Ar fraction in the H-mode at the same high rf power 700 W, at which molecular chlorine dissociation is nearly complete; this value of $b_{Cl,Xe}$ is used to determine n_{Cl} at all other powers. The energy threshold for electron impact excitation of ground state Cl to the excited state is 10.50 eV and, as such, is an even better match for Xe actinometry at 828.0 nm than is Cl₂, ensuring that $b_{Cl,Xe}$ is relatively independent of T_e . Using the values for $b_{Cl,Xe}, b_{Cl_2 \rightarrow Cl,Xe}$ (discussed below), and Eq. (5) yields the absolute Cl densities also shown in Fig. 2.

B. Proportionality constant $b_{Cl_2 \rightarrow Cl,Xe}$ and rate constant for $Cl_2 + e^- \rightarrow Cl + Cl^* + e^-$

Figure 3 shows n_{Cl} in the E-mode for a 1% Ar Cl₂-Ar discharge assuming $K_{Cl_2 \rightarrow Cl + Cl^*} = 0$ (i.e., $b_{Cl_2 \rightarrow Cl,Xe} \rightarrow \infty$). The Cl number density is determined to be $\sim 1.2 \times 10^{14} \text{ cm}^{-3}$ in the limit of zero rf power, corresponding to a $\sim 10\%$ dissociation of Cl₂. This value is expected to be $< 1\%$, however. This discrepancy is a consequence of reaction (7). To assess the contribution of this reaction to the Cl* density, the rate constant $K_{Cl_2 \rightarrow Cl + Cl^*}$ was estimated by assuming an exponential dependence of the form $A_0 \exp(-12.98/T_e)$. The 12.98 eV energy threshold, E_T , is chosen to equal the minimum energy required to dissociate Cl₂ to

yield two ground state Cl atoms (2.48 eV) and to excite one of these to the $4p^2D^0J' = 3/2$ excited state (10.5 eV). [E_T may, in fact, exceed this 12.98 eV value because the Franck-Condon factors for reaction (7) may yield an energy barrier larger than E_T and the density of final states factor increases significantly a few eV above E_T .] Since the rate constant for the electronic impact excitation of ground state Xe to the $2p_5$ Paschen level, $K_{Xe}, \sim 6 \times 10^{-11} \text{ cm}^3 \text{ s}^{-1}$ for $T_e = 3.0 \text{ eV}$,²¹ it is highly unlikely that the electron impact dissociative excitation cross section for reaction (7) exceeds K_{Xe} . $b_{Cl_2 \rightarrow Cl,Xe}$ is determined by computing K_{Xe} and $K_{Cl_2 \rightarrow Cl + Cl^*}$ by the following approach. For each Cl₂ fraction, A_0 is varied while the atomic chlorine densities are recalculated including the contribution from reaction (7) until $n_{Cl} \rightarrow \sim 0 \text{ cm}^{-3}$ in the limit of 0 W rf power, as is shown in Fig. 3. This iterative

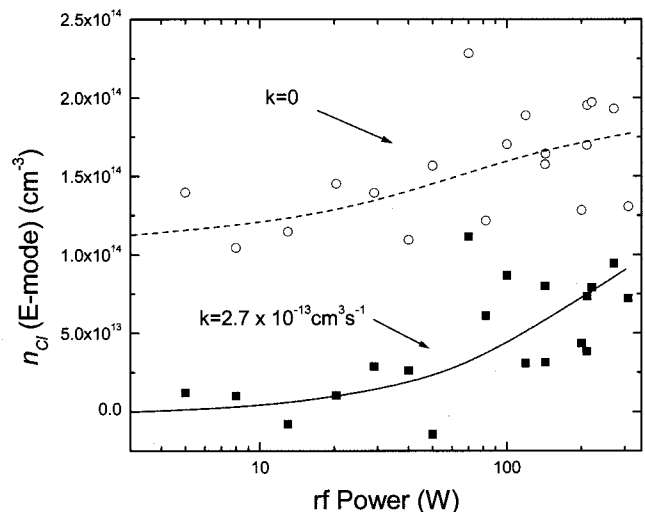


FIG. 3. Absolute densities of Cl vs rf power in the E-mode of an 18 mTorr 1% Ar Cl₂-Ar ICP plasma with 5% of the trace rare gas mixture. Densities are determined assuming two different values of the rate constant, $K_{Cl_2 \rightarrow Cl + Cl^*}$, for the dissociative excitation of Cl₂ to Cl + Cl*.

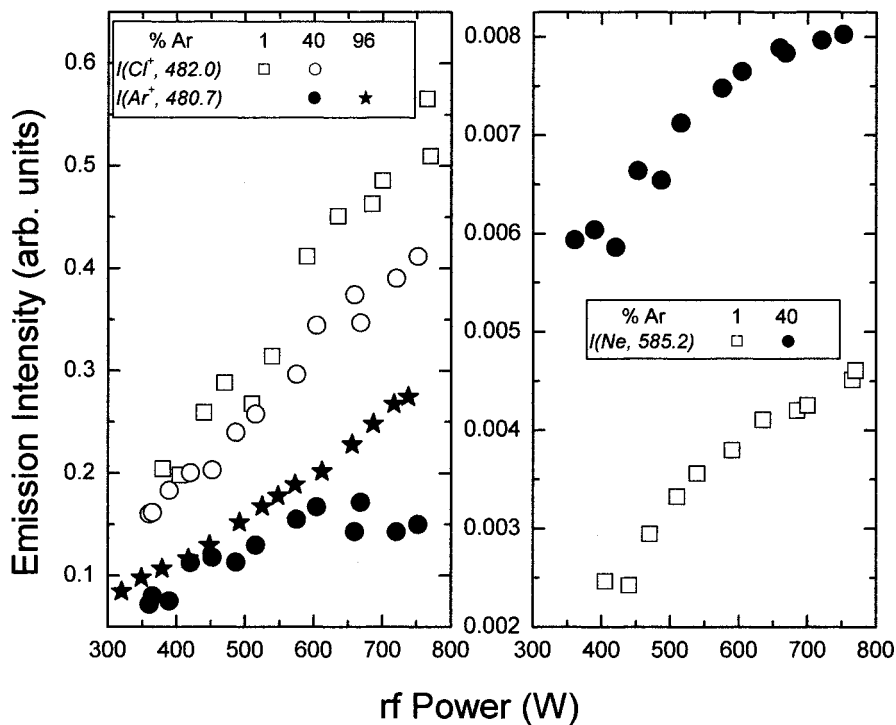
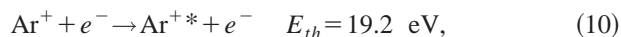
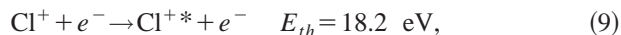


FIG. 4. Optical emission intensity vs rf power and Ar fraction (1%, 40%, and 96%) for (a) the Cl⁺ emission line at 482.0 nm and the Ar⁺ emission line at 480.7 nm, and (b) the Ne emission line at 585.2 nm, in an 18 mTorr Cl₂-Ar ICP plasma with 5% of the trace rare gas mixture. Data have been corrected for the wavelength-dependent response of the spectrometer and photomultiplier tube. Data from the 13% and 78% Ar mixtures have not been plotted here.

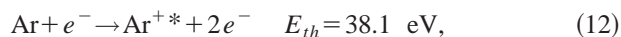
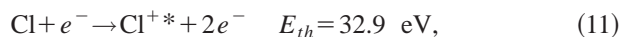
process for each of the four Cl₂ fractions studied yields $A_0 = 1.7 \pm 1.0 \times 10^{-11} \text{ cm}^3 \text{ s}^{-1}$. Thus, for typical plasma electron temperatures of 3–5 eV, the rate constant for reaction (7) is predicted to be $\sim 10^{-13} \text{ cm}^3 \text{ s}^{-1}$. Reaction (7) impacts the determination of n_{Cl} in the *E*-mode (Fig. 2); it has negligible effect in the *H*-mode.

C. Cl⁺, Ar⁺, and Ne emission and absolute densities for Cl⁺ and Ar⁺

The integrated emission intensities from Cl⁺ at 482.0 nm and Ar⁺ at 480.7 nm, corresponding to the respective transitions $3p^3 4p^3 F \rightarrow 3d^3 F^0$ and $3p^4 4p^4 P^0 \rightarrow 4s^4 P$, are shown in Fig. 4. Also included in Fig. 4 are the integrated emission intensities from Ne at 585.2 nm. This Cl⁺ and Ar⁺ emission most likely occurs by the following pathways:



where Cl⁺* and Ar⁺* are the Cl⁺($3p^3 4p^3 F$) and Ar⁺($3p^4 4p^4 P^0$) excited states. These emitting states are produced by a two-step process, the first of which is ionization. Alternatively, these excited states could be produced from the single-step electron impact ionization and excitation of ground state Cl and Ar:



Determining positive ion densities using this actinometry method is useful only if the density of excited ions produced by the two-step route of reaction (9) [or (10)] is comparable to or greater than that produced by this one-step route of

reaction (11) [or (12)]. This depends on the excitation cross section of each reaction, the electron density, and the electron energy distribution function (EEDF). As is seen below, deviations from a Maxwellian distribution can be important. The relative importance of these alternative routes is now assessed.

If the normalized EEDF does not change with rf power and the electron density is proportional to rf power ($n_{\text{Cl}} \sim 0$ in the *H*-mode), the emission intensity from X⁺* produced by a two-step process would increase quadratically with rf power, while that from a one-step process would increase linearly. Figure 4 shows variations with rf power that are intermediate between linear and quadratic for both Cl⁺* and Ar⁺* emission. While this might seem to indicate that the one-step process is partly responsible for the ionic emission, other evidence discussed below suggests that this is not the case. Instead, the increase in T_e with increasing power, especially for Ar-rich plasmas,²⁰ is likely responsible for this subquadratic behavior.

Zapesochnyi *et al.*²⁵ measured a peak value of $5 \times 10^{-18} \text{ cm}^2$ for Ar⁺ excitation by reaction (10) near threshold ($\sim 19 \text{ eV}$) and Griffin *et al.*,²⁶ using close-coupling *R*-matrix theory, calculated a peak cross section value of $\sim 1.2 \times 10^{-17} \text{ cm}^2$ for this process also at $\sim 19 \text{ eV}$. Latimer and St. John,²⁷ Van Zyl *et al.*,²⁸ Clout and Heddle,²⁹ and Bogdanova and Yurgenson³⁰ have measured the cross section for excitation to Ar⁺* from Ar in reaction (12); all report a peak value $\sim 3.4 \times 10^{-19} \text{ cm}^2$ at 54 eV.

Electron temperatures in these Cl₂-Ar plasmas have been measured by the authors using trace rare gases optical emission spectroscopy and are reported elsewhere.²⁰ For “neat” Ar plasmas, T_e is $\sim 6 \pm 2 \text{ eV}$ at an Ar pressure of 18 mTorr and a density of $3 \times 10^{14} \text{ cm}^{-3}$ estimated for the hot plasma gas at 600 W. This electron temperature is mostly

characteristic of the EEDF above ~ 10 eV, although it also senses lower energy electrons that excite emission from metastable levels. From a global model analysis, we estimate a T_e of 2.8 eV for the same conditions,³¹ which is characteristic of even higher energy electrons, with energies above the ionization potential of Ar (15.76 eV). Using cross sections reported in Refs. 25 and 27, the above Ar density of 3×10^{14} cm⁻³ and the Ar⁺ density of 6×10^{10} cm⁻³ (from Fig. 6), the rate of reaction (12) producing Ar⁺* is 0.09 and $6.72 \times$ that for reaction (10) for $T_e = 2.8$ and 6.0 eV, respectively. They are equal for $T_e = 4.2$ eV. The relative importance of the two routes is clearly very sensitive to T_e .

However, it has been shown that EEDFs of similar Ar plasmas exhibit a suppressed tail at energies above the plasma potential,^{32,33} mostly because these high energy electrons are not confined by the sheath potentials and are therefore rapidly lost at the walls. Singh and Graves measured EEDFs in Ar ICPs above the plasma potential.³⁴ For 10 mTorr, their EEDF can be fit to a temperature of ~ 3.8 eV for $E < 15$ eV and 1.5 eV for $E > 15$ eV. For 40 mTorr, $T_e = 2.2$ eV fits $E < 13$ eV, and 1.7 eV for $E > 13$ eV. We therefore assume that for our 18 mTorr plasma, T_e is 3.4 and 1.6 eV, below and above the plasma potential (~ 20 eV), respectively. Using cross sections reported in Refs. 25 and 27, we first assume that reactions (10) and (12) thresholds (19.2 and 38.1 eV, respectively) are both in the high energy tail which is described by $T_e = 1.6$ eV; then reaction (12) produces Ar⁺* $0.0002 \times$ as fast as reaction (10). If the plasma potential is 25 or 30 eV, this ratio increases to 0.008 or 0.06, respectively, and reaction (10) is still dominant.

Analysis of the $I(\text{Ar},480.7)/I(\text{Ne},585.2)$ emission ratio also provides information about the high-energy tail of the EEDF. The pathway for the Ne 585.2 nm emission is one-step electron impact excitation from the ground state to the $2p_1$ Paschen level, which is 18.9 eV above the ground state. The $1s_3$ and $1s_5$ Ne metastable concentrations in these plasmas are too small relative to the ground state Ne for the alternative metastable excitation pathway to be significant.^{35,36} Using the cross sections in Refs. 25 and 27 and those reported by Register *et al.*³⁷ and Chilton *et al.*³⁸ for Ne $2p_1$ excitation, this emission ratio is computed as a function of T_e , assuming Ar⁺* emission originates either from only reaction (10) or (12). These computed ratios are presented in Fig. 5 for the experimental Ar–Ne input flow ratio of 96:1. If all the Ar⁺ emission arises from reaction (12), this computed emission ratio of 1×10^{-5} at $T_e = 1.6$ eV is well below the observed emission ratio of 0.06–0.08 in the *H*-mode; it is still much smaller at higher T_e (< 3 eV). This is further evidence that excitation via reaction (12) contributes insignificantly to the population of the Ar⁺* state.

Ne emission at 585.2 nm is detected in the *E*-mode at ~ 10 W for all Ar fractions, while no Ar⁺* emission is observed under these same conditions. (The observation of this Ne emission suggests a bulk electron temperature of at least ~ 3.5 eV, given an electron density of $\sim 1 \times 10^9$ cm⁻³.¹⁹) Since $n_{\text{Ar}^+}/n_{\text{Ar}}$ is much smaller in the *E*-mode (Ar and Ar⁺ densities are $\sim 5 \times 10^{14}$ and $\ll 10^{10}$ cm⁻³, respectively, for a 96% Ar plasma at 10 W) than in the *H*-mode and the electron temperatures are likely higher in the *H*-mode, this observa-

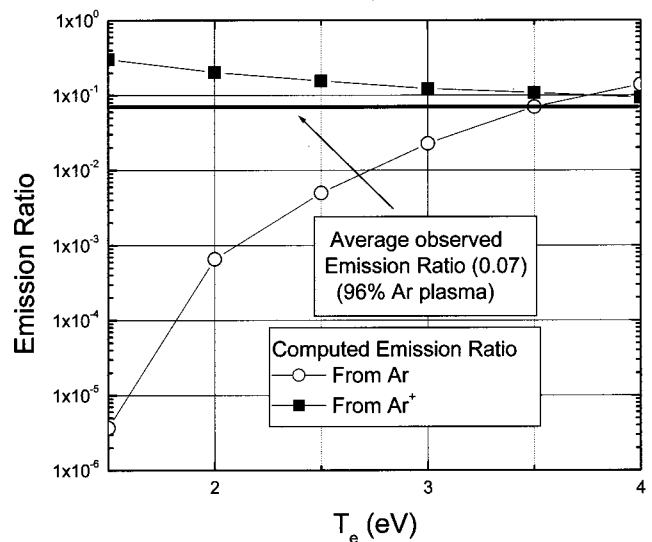


FIG. 5. Computed emission ratio of $I(\text{Ar}^+,480.7)/I(\text{Ne},585.2)$ assuming Ar⁺ emission originates only from electron impact of either Ar or Ar⁺ vs electron temperature (T_e) in an 18 mTorr Cl₂–Ar ICP plasma (96% Ar) with 5% of the trace rare gas mixture. The averaged observed emission ratio (0.07) after spectral calibration is also shown for reference.

tion also suggests that in the *H*-mode the EEDF is depleted above 19 eV, has an effective $T_e < 2.0$ eV, and the emission from Ar⁺* originates from reaction (10).

A similar analysis to determine the source(s) of Cl⁺* emission at 482.0 nm is more uncertain because the cross sections for reactions (9) and (11) have not been reported. We estimate their rate coefficients by assuming that the cross sections for these reactions have the same shape and peak values as those for reactions (10) and (12), with energies downshifted by 1.0 and 5.16 eV, the differences in their respective threshold energies. This seems reasonable, given the almost identical electron impact ionization cross sections of Cl and Ar measured by Hayes *et al.*³⁹ and Wetzel *et al.*⁴⁰ For a 95% Cl₂ plasma, Cl₂ is nearly completely ($\sim 80\%$) dissociated into Cl atoms present at a density of $\sim 8 \times 10^{14}$ cm⁻³. Reference 41 reported bi-Maxwellian distributions in a Cl₂ ICP for 10 and 20 mTorr at rf power densities similar to those used here, with breaks at ~ 11 and 9 eV, respectively. Using their data, T_e is estimated to be 2.80 eV at lower energies and 1.95 eV at higher energies. For $T_e = 1.95$ eV, reaction (11) is 0.012 \times that of reaction (9). Also, the computed emission ratio $I(\text{Cl}^+,482.0)/I(\text{Ne},585.2)$ is 3.6×10^{-4} for $T_e = 1.95$ eV, assuming Cl⁺* emission originates only from reaction (11). This is again much less than the observed ratio of 0.1–0.3, suggesting a negligible fraction of the emission originated from reaction (11).

Therefore, the Cl⁺* and Ar⁺* emissions in “neat” Cl₂ and Ar plasmas seem to originate from reactions (9) and (10), and not reactions (11) and (12). Since T_e varies smoothly in Cl₂/Ar mixtures from “neat” Cl₂ to Ar plasmas,²⁰ this conclusion seems reasonable for each mixture. Then n_{Cl^+} and n_{Ar^+} can be expressed as

$$n_{\text{Cl}^+} = b_{\text{Cl}^+, \text{Ne}} n_{\text{Ne}}^0 \delta(T_g, T_w) \frac{I(\text{Cl}^+, 482.0)}{I(\text{Ne}, 585.2)}, \quad (13)$$

TABLE II. Calibration constants determined in the actinometry analysis.

% Ar	$b_{\text{Cl}^+,\text{Ne}}$	$b_{\text{Ar}^+,\text{Ne}}$	$T_e(\text{eV})^a$
1	25.3	9.3	4.0
13	24.8	9.2	4.1
40	23.8	9.1	4.3
78	22.6	7.2	5.5
96	16.7	6.7	6.0

^a T_e from Ref. 20.

$$n_{\text{Ar}^+} = b_{\text{Ar}^+,\text{Ne}} n_{\text{Ne}}^0 \delta(T_g, T_w) \frac{I(\text{Ar}^+, 480.7)}{I(\text{Ne}, 585.2)}. \quad (14)$$

The energy thresholds for the excited states of Cl^+ and Ar^+ are 18.2 and 19.2 eV, respectively, so the $2p_1$ Paschen level of Ne, 18.9 eV above its ground state, is an excellent actinometer for both lines. The proportionality constant $b_{\text{Ar}^+,\text{Ne}}$ is the ratio of the excitation rate of Ne^* to Ar^+* determined from cross sectional data from Chilton *et al.*³⁸ and Latimer and St. John,²⁷ respectively. These values are also given in Table II for the conditions used in this study. The relatively small decrease (1.38-fold) in $b_{\text{Ar}^+,\text{Ne}}$ as the plasma changes from Cl dominant (1% Ar) to Ar dominant (78% Ar) justifies using Ne emission actinometry at 585.2 nm to determine Ar^+ absolute densities.

Since cross sections are not available for reaction (9), we computed the proportionality constant $b_{\text{Cl}^+,\text{Ne}}$ in Eq. (13) by a different method. Figure 2 reveals that Cl_2 is $\sim 90\%$ dissociated for a “pure” chlorine discharge (1% Ar) at rf powers > 600 W. Cl_2^+ and Cl^- concentrations are much less than Cl^+ under these conditions,^{17,18} so $n_{\text{Cl}^+} \approx n_e$. With our previously reported measurements of n_e in an 18 mTorr Cl_2 discharge as a function of rf power made by microwave interferometry,⁴² we use $n_{\text{Cl}^+} \approx n_e$ to determine $b_{\text{Cl}^+,\text{Ne}}$ from Eq. (13) for the

Cl_2 plasma. Since the energy difference between the thresholds for electron impact excitation of the $2p_1$ Paschen level of Ne and the Cl^+* excited state is small (0.7 eV), we expect a weak variation of $b_{\text{Cl}^+,\text{Ne}}$ with changes in T_e , as the rf power and Ar fraction are varied. Using the energy-shifted cross sections described above, $b_{\text{Cl}^+,\text{Ne}}$ is estimated to decrease by a factor of 1.5 as the plasma changes from Cl_2 dominant (1% Ar) to Ar dominant (78% Ar). These values of $b_{\text{Cl}^+,\text{Ne}}$ are given in Table II. The Cl^+ and Ar^+ densities obtained from Eqs. (13) and (14) are presented in Fig. 6.

IV. DISCUSSION

A. Cl_2 and Cl densities

Figure 2 shows that for an rf power of 600 W, n_{Cl_2} decreases by a factor of 10 from ~ 6 to $\sim 0.6 \times 10^{13} \text{ cm}^{-3}$ as the Ar input flow fraction is increased from 1% (95% Cl_2) to 78% (18% Cl_2). For the same increase in Ar fraction, n_{Cl} decreases by a factor of ~ 3 from ~ 7.5 to $\sim 2.5 \times 10^{14} \text{ cm}^{-3}$. The anticipated increase in n_{Cl} and decrease in n_{Cl_2} as rf power is increased from ~ 350 to ~ 750 W is also observed for all Ar fractions.

Cl_2 and Cl actinometry, mass balance, and the data shown in Fig. 2 are used to determine the Cl_2 percent dissociation, $D_\%$, vs Ar fraction for 600 W (see Fig. 7). $D_\%$ is defined as

$$D_\% = \frac{n_{\text{Cl}}(\text{rf power, Ar fraction})}{2 \delta(T_g, T_w) n_{\text{Cl}_2}^0(\text{Ar fraction})} \times 100. \quad (15)$$

The gas dissociation increases from 78% to 96% as the Ar fraction is increased from 1% to 78%. Also, the power density at which the gas is “completely” dissociated (defined here as $\sim 90\%$) decreases with increasing Ar fraction. These

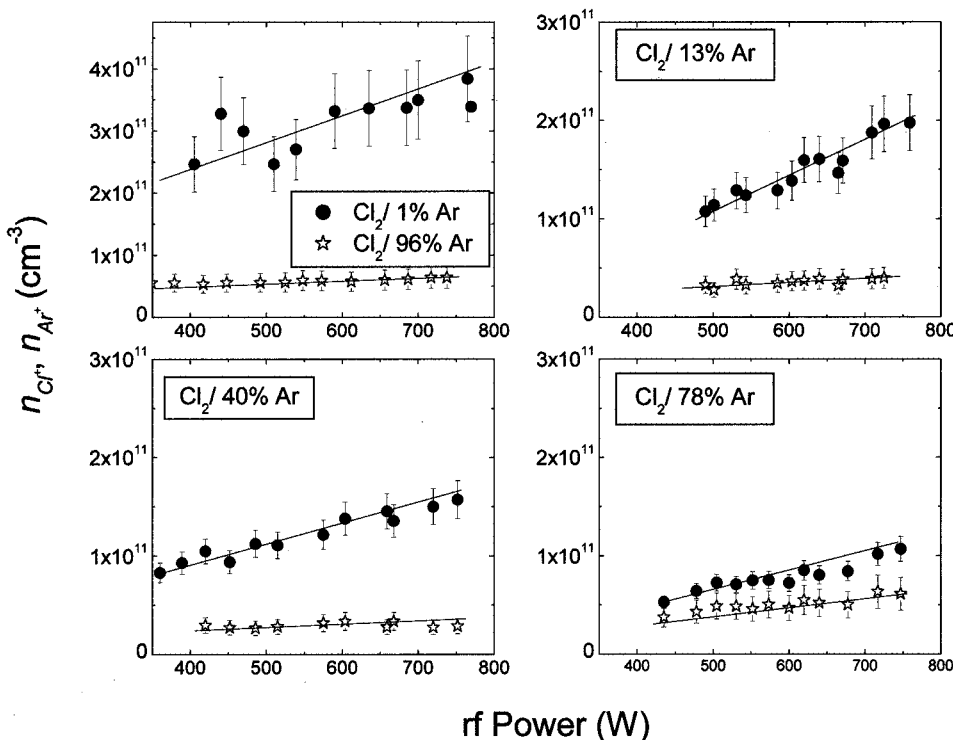


FIG. 6. Absolute densities of Cl^+ (solid symbols) and Ar^+ (open symbols) vs rf power and Ar fraction (1%, 13%, 40%, 78%, and 96%) in an 18 mTorr Cl_2 -Ar ICP plasma with 5% of the trace rare gas mixture. The Cl^+ densities for Cl_2 plasmas and Ar^+ densities for Ar plasmas are both plotted in the upper left panel. A line fit to aid viewing has been added.

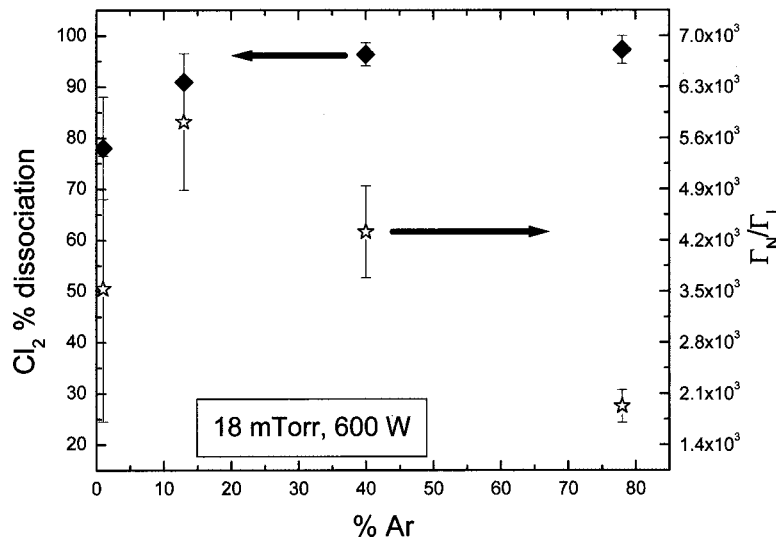


FIG. 7. Percentage dissociation of Cl₂ and the neutral (Cl and Cl₂) to ion (Cl⁺ and Ar⁺) flux ratio vs Ar fraction (1%, 13%, 40%, and 78%) in an 18 mTorr Cl₂-Ar ICP plasma at 600 W with 5% of the trace rare gas mixture.

interrelated observations arise from the increase in T_e from ~4.0 to 5.5 eV as the Ar fraction is increased from 1% to 78%.²⁰

Given the high electron temperatures, Cl is primarily generated by the electron dissociation of Cl₂ as opposed to dissociative attachment.²³ Using a zero-order global model, n_{Cl} is

$$n_{Cl} = \frac{2k_{diss}n_{Cl_2}^0n_e}{k_r}, \quad (16)$$

where k_{diss} is the dissociation rate constant of Cl₂ [$=4.52 \times 10^{-8} \exp(-7.40/T_e)$ cm³ s⁻¹],²² $k_r (=2\gamma D_{eff}/l_{eff}^2)$ is the Cl-atom recombination rate constant, γ is the Cl wall recombination coefficient, D_{eff} is an effective diffusion coefficient for Cl transport to the walls that combines a molecular diffusion coefficient and a pressure-dependent Knudsen diffusion coefficient (1.4×10^4 cm² s⁻¹),⁴³ and l_{eff} is the effective diffusion length approximately given by the plasma volume-to-surface area ratio (2.1 cm). Thus at 600 W, we estimate γ using data presented in Figs. 2 and 6 and Eq. (16), obtaining an average value of 0.29, which is in good agreement with that measured by Kota *et al.*⁴⁴ (0.5) but much higher than that measured by Malyshev *et al.* (0.03).²² The difference with Ref. 22 can probably be attributed to the factor of ~3× larger rf power density and smaller reactor volume in the current ICP that results in a reduction of wall passivation due to rapid ion bombardment. Using this expression in Eq. (15) for n_{Cl} , then $D_{\%} \propto k_{diss}n_e/\delta(T_g, T_w)$. With the increase in T_e as the Ar fraction increases from 1% to 78%, k_{diss} increases from 0.7 to 1.2×10^{-8} cm³ s⁻¹, n_e decreases from ~3.0 to $\sim 1.4 \times 10^{11}$ cm⁻³, and $\delta(T_g, T_w)$ decreases²³ by an approximate factor of 1.7. This results in a factor of ~1.36 increase in $D_{\%}$ in good agreement with the factor of ~1.23 increase determined using actinometry.

Also shown in Fig. 7 are the associated errors in the computed $D_{\%}$ for each of the four Ar fractions. The extremes of the error bars indicate the difference in $D_{\%}$ from Cl₂ actinometry versus Cl actinometry with mass balance. The two

actinometric techniques agree within 6% (for a 13% Ar plasma) to 25% (1% Ar plasma) and, thus, together provide reasonably accurate measurements of atomic and molecular chlorine densities.

B. Positive ion densities

Figure 6 shows that for each of the four Ar fractions, n_{Cl^+} roughly doubles as rf power is doubled, whereas n_{Ar^+} increases sublinearly with power. As expected, n_{Ar^+} increases and n_{Cl^+} decreases as the Ar fraction increases. However, $n_{Ar^+} < n_{Cl^+}$ even for the largest Ar fraction studied (78%), for which $n_{Ar^+} \sim 2.3 n_{Cl^+}$. The dominance of Cl⁺ in Ar-rich plasmas is likely due to the lower ionization potential for Cl (12.97 eV) compared with that for Ar (15.76 eV).

Assuming similar loss processes for Ar⁺ and Cl⁺ (diffusion to the sheath edge), one expects

$$\frac{n_{Ar^+}}{n_{Cl^+}} \approx \frac{k_{iz(Ar)}n_{Ar}}{k_{iz(Cl)}n_{Cl}}, \quad (17)$$

where k_{iz} is the ionization rate constant. The difference between the experimentally determined quantities on the left- and right-hand sides of Eq. (17) decreases from ~30% to <1% as the Ar fraction increases from 13% to 78%, because the S/N ratio of the Ne 585.2 nm emission line increases from ~2:1 to ~50:1 over the same range due to the increase in T_e . Thus, the absolute certainty in Cl⁺ and Ar⁺ number densities improves for increasing Ar fractions. These data may also suggest a depleted tail in the EEDF. At 600 W, n_{Cl^+} decreases from 3.0 to 0.8×10^{11} cm⁻³ as the Ar fraction is increased from 1% to 78%, which roughly matches the same proportional decrease in n_{Cl} (Fig. 2). A slower decrease in n_{Cl^+} would be expected due to the concomitant increase in T_e and supposed doubling in the density of high-energy (>13 eV) electrons from 1.6 to 2.7×10^{10} cm⁻³ for a Maxwellian EEDF. While this could suggest a possible tapering of the high-energy tail of the EEDF above ~13 eV, it is more likely due to a stronger dependence of the determined acti-

nometry constant $b_{\text{Cl}^+, \text{Ne}}$ with electron temperature than that predicted in Table II, given the uncertainty in the Cl^{+*} cross section.

Figure 6 shows that n_{Ar^+} increases by only a factor of ~ 1.2 for all Ar fractions from ~ 350 to ~ 750 W. This suggests a depletion of the high-energy tail of the EEDF above ~ 16 eV, due to significant inelastic scattering of these high-energy electrons with Ar atoms and electron loss to the walls.^{45–49} At 600 W, n_{Ar^+} increases only from ~ 4.0 to $\sim 7.0 \times 10^{10} \text{ cm}^{-3}$ as n_{Ar} increases from 7.0×10^{13} (13% Ar) to $5.4 \times 10^{14} \text{ cm}^{-3}$ (96% Ar). This is further evidence for a depleted high-energy tail of the EEDF, even though T_e increases with increasing Ar fraction.²⁰

The net positive ion density, n_{i^+} , ($\approx n_{\text{Cl}^+} + n_{\text{Ar}^+}$) decreases from 3.0 to $1.4 \times 10^{11} \text{ cm}^{-3}$ as the plasma changes from Cl (1% Ar) to Ar-rich (96% Ar). This variation is similar to that of Eddy *et al.*¹⁵ who showed that the plasma density ($n_e \approx n_{i^+}$) in the processing region of a 1 mTorr ECR discharge decreases from 2.5 to $1.5 \times 10^{10} \text{ cm}^{-3}$ as the Ar fraction increases from 25% to 85%.

C. Neutral flux-to-ion flux ratio

The neutral to ion flux ratio to the surface, Γ_N/Γ_I , provides a measure of the competition between surface chlorination and sputtering during etching. This ratio is approximately equal to

$$\frac{\Gamma_N}{\Gamma_I} \approx \frac{n_{\text{Cl}} + n_{\text{Cl}_2}}{n_{\text{Cl}^+} + n_{\text{Ar}^+}} \quad (18)$$

and (the right-hand side) is presented in Fig. 7 using the data in Figs. 2 and 6. The numerator in Eq. (18) is the sum of the densities of all the dominant neutral species that chemically react with a semiconductor surface (Si, III–V) to form the adlayer during etching (chlorination). Similarly, the denominator in this equation is the sum of the densities of the dominant positive ions that can physically sputter (desorb) the adlayer formed during chlorination and should be proportional to the total sputtering rate, since the sputtering rates of Cl^+ and Ar^+ are expected to be comparable. [Rigorously, the velocities to the surface must be included to relate each particle density to its flux contribution in Eq. (18). In the *H*-mode, the density of Cl dominates the numerator, so the different Cl and Cl_2 velocities to the surface are not significant. The larger Cl density and reactivity make it the dominant chlorination reactant. The velocities of Cl^+ and Ar^+ are about the same, and are about equal to that of Cl in the bulk of the plasma. Also, the ion flux into the sheath is the same as that hitting the surface in steady state.]

Figure 6 shows that n_{Cl^+} decreases from 1.5 to $\sim 1.0 \times 10^{11} \text{ cm}^{-3}$ and n_{Ar^+} increases from ~ 4.0 to $\sim 7.0 \times 10^{10} \text{ cm}^{-3}$ as the Ar fraction increases from 13% to 78%, so the positive ion density decreases by a factor of 1.2 from 1.8 to $1.4 \times 10^{11} \text{ cm}^{-3}$. Figure 2 shows that n_{Cl} decreases by a larger factor, ~ 3.2 , from ~ 8.0 to $\sim 2.5 \times 10^{14} \text{ cm}^{-3}$ over the same Ar fraction range. Consequently, there is a decrease in Γ_N/Γ_I from $\sim 5.8 \times 10^3$ to $\sim 1.9 \times 10^3$ as the Ar content increases at 600 W (Fig. 7). There is some uncertainty about the trend for Ar fractions between 1% and 13%.

The need for an increased sputtering rate *vis-à-vis* chlorination rate for efficient etching is suggested by the studies of etching of InN and GaN in a Cl_2 -Ar ICP in which the etching rates were found to peak for Ar fractions of $\sim 90\%$.⁷ InP etching showed little dependence on the Ar fraction, while GaP etching was the fastest for an Ar fraction of 10%.⁸ It seems that in these two systems there is less need for enhanced sputtering during etching.

V. CONCLUSIONS

Cl_2 -Ar ICPs were investigated by rare gas actinometry using optical emission spectroscopy. Cl_2 and Cl absolute ground state densities were obtained from Cl_2 and Cl integrated emission intensities at 306.0 and 822.2 nm, respectively, coupled with Xe actinometry at 828.0 nm, and modeling. Cl^+ and Ar^+ absolute densities were obtained from Cl^+ and Ar^+ emission intensities at 482 and 480.7 nm, respectively, combined with Ne actinometry at 585.2 nm and microwave interferometry. The contribution of one-step excitation of Cl and Ar to produce Cl^{+*} and Ar^{+*} was determined to be unimportant. For 600 W (10.6 W cm^{-2} , 0.7 W cm^{-3}), the percent dissociation of Cl_2 was found to increase with Ar content from 78% for a chlorine dominant (1% Ar) discharge to 96% for an Ar dominant (78% Ar) discharge. Under the same conditions, the total positive ion density ($n_{\text{Cl}^+} + n_{\text{Ar}^+}$) was found to decrease from 1.8 to $1.4 \times 10^{11} \text{ cm}^{-3}$ as the Ar fraction was increased from 13% to 78%. Thus, the neutral to ion flux ratio is strongly dependent on Ar fraction, decreasing from ~ 5.8 to $\sim 1.9 \times 10^3$ over the same Ar fraction range, with the change in atomic Cl density being the dominant factor. Cl emission at 822.2 nm and Xe emission at 828.0 nm were used to show that dissociative excitation of Cl_2 to Cl^* contributes significantly to Cl emission at 822.2 nm in the *E*-mode. The rate constant for this process is $1.7 \pm 1.0 \times 10^{-11} \exp(-12.98/T_e) \text{ cm}^3 \text{ s}^{-1}$.

Future studies will explore the relative rates of surface chlorination and sputtering during the etching of III–V semiconductors in Cl_2 -Ar discharges by using etch rate measurements combined with the plasma densities measured here and laser desorption to probe the surface adlayer.^{19,42}

ACKNOWLEDGMENTS

The NSF Grant No. DMR-98-15846 supported the activities of two of the authors (N.C.M.F. and I.P.H.) in this work. The authors would like to thank Andy Miller for his assistance in coding and conducting some of the data analysis.

¹ *Quantum Well Lasers*, edited by P. S. Zory (Academic, San Diego, CA, 1995).

² S. Nakamura, T. Mukai, and M. Senoh, *Appl. Phys. Lett.* **64**, 1687 (1994).

³ S. Nakamura, M. Senoh, and T. Mukai, *Appl. Phys. Lett.* **62**, 2390 (1993).

⁴ J. B. Limb, H. Xing, B. Moran, L. McCarthy, S. P. DenBaars, and U. K. Mishra, *Appl. Phys. Lett.* **76**, 2457 (2000).

⁵ M. Asif Khan, A. Bhattacharai, J. N. Kunzia, and D. T. Olson, *Appl. Phys. Lett.* **63**, 1214 (1993).

⁶ R. J. Shul, A. J. Howard, C. B. Vartuli, P. A. Barnes, and W. S. Seng, *J. Vac. Sci. Technol. A* **14**, 1102 (1993).

⁷ Y. Hahn, D. C. Hays, S. M. Donovan, C. R. Abernathy, J. Han, R. J. Shul,

- H. Cho, K. B. Jung, and S. J. Pearton, *J. Vac. Sci. Technol. A* **17**, 768 (1999).
- ⁸R. J. Shul, G. B. McClellan, R. D. Briggs, R. D. Rieger, S. J. Pearton, C. R. Abernathy, J. W. Lee, C. Constantine, and C. Barratt, *J. Vac. Sci. Technol. A* **15**, 633 (1997).
- ⁹F. Ren, W. S. Hobson, J. R. Lothian, J. Lopata, J. A. Caballero, S. J. Pearton, and M. W. Cole, *Appl. Phys. Lett.* **67**, 2497 (1995).
- ¹⁰J. W. Lee, J. Hong, C. R. Abernathy, E. S. Lambers, S. J. Pearton, W. S. Hobson, and F. Ren, *J. Vac. Sci. Technol. A* **14**, 2567 (1996).
- ¹¹H. Cho, Y. B. Hahn, D. C. Hays, C. R. Abernathy, S. M. Donovan, J. D. MacKenzie, S. J. Pearton, J. Han, and R. J. Shul, *J. Vac. Sci. Technol. A* **17**, 2202 (1999).
- ¹²G. Franz and F. Rinner, *J. Vac. Sci. Technol. A* **17**, 56 (1999).
- ¹³W. J. Lee, H. S. Kim, G. Y. Yeom, J. W. Lee, and T. I. Kim, *J. Vac. Sci. Technol. A* **17**, 1230 (1999).
- ¹⁴A. T. Ping, C. Youtsey, I. Adesida, M. Asif Khan, and J. N. Kuzina, *J. Electron. Mater.* **24**, 229 (1995).
- ¹⁵C. R. Eddy, Jr., D. Leonhardt, S. R. Douglass, B. D. Thomas, V. A. Shamamian, and J. E. Butler, *J. Vac. Sci. Technol. A* **17**, 38 (1999).
- ¹⁶J. W. Coburn and M. Chen, *J. Appl. Phys.* **51**, 3134 (1980).
- ¹⁷M. V. Malyshev, N. C. M. Fuller, K. H. A. Bogart, V. M. Donnelly, and I. P. Herman, *J. Appl. Phys.* **88**, 2246 (2000).
- ¹⁸M. V. Malyshev, N. C. M. Fuller, K. H. A. Bogart, V. M. Donnelly, and I. P. Herman, *Appl. Phys. Lett.* **74**, 1666 (1999).
- ¹⁹J. Y. Choe, I. P. Herman, and V. M. Donnelly, *J. Vac. Sci. Technol. A* **15**, 3024 (1997).
- ²⁰N. C. M. Fuller, V. M. Donnelly, and I. P. Herman (unpublished).
- ²¹J. T. Fons and C. C. Lin, *Phys. Rev. A* **58**, 4603 (1998).
- ²²M. V. Malyshev and V. M. Donnelly, *J. Appl. Phys.* **88**, 6207 (2000).
- ²³V. M. Donnelly and M. V. Malyshev, *Appl. Phys. Lett.* **77**, 2467 (2000).
- ²⁴Reference 23 determined a square root dependence of gas temperature with rf power, but since this dependence may be very reactor specific and the power density in this reactor is $\sim 3\times$ that in Ref. 23, a linear dependence was assumed here.
- ²⁵P. Zapesochnyi, A. I. Imre, A. I. Dashchenko, V. S. Vukstich, F. F. Danch, and V. A. Kel'man, *Sov. Phys. JETP* **36**, 1056 (1973).
- ²⁶D. C. Griffin, M. S. Pindzola, J. A. Shaw, N. R. Badnell, M. O'Mullane, and H. P. Summers, *J. Phys. B* **30**, 3543 (1997).
- ²⁷I. D. Latimer and R. M. St. John, *Phys. Rev. A* **1**, 1612 (1970).
- ²⁸B. Van Zyl, G. H. Dunn, G. Chamberlain, and D. W. O. Heddle, *Phys. Rev. A* **22**, 1916 (1980).
- ²⁹P. N. Clout and D. W. O. Heddle, *J. Phys. B* **4**, 483 (1971).
- ³⁰I. P. Bogdanova and S. V. Yurgenson, *Opt. Spectrosc.* **62**, 21 (1987).
- ³¹Global model analysis to yield tail temperature of 2.8 eV.
- ³²S.-H. Seo, J.-I. Hong, and H.-Y. Chang, *Appl. Phys. Lett.* **74**, 2776 (1999).
- ³³V. A. Godyak, R. B. Piejak, and B. M. Alexandrovich, *Plasma Sources Sci. Technol.* **4**, 332 (1995).
- ³⁴H. Singh and D. Graves, *J. Appl. Phys.* **88**, 3899 (2000).
- ³⁵M. H. Phillips, L. W. Anderson, and C. C. Lin, *Phys. Rev. A* **323**, 2117 (1985).
- ³⁶J. Boffard and C. C. Lin (private communication).
- ³⁷D. F. Register, S. Trajmar, G. Steffensen, and D. C. Cartwright, *Phys. Rev. A* **29**, 1793 (1984).
- ³⁸J. E. Chilton, M. D. Stewart, Jr., and C. C. Lin, *Phys. Rev. A* **61**, 052708 (2000).
- ³⁹T. D. Hayes, R. C. Wetzel, and R. S. Freund, *Phys. Rev. A* **35**, 578 (1987).
- ⁴⁰R. C. Wetzel, F. A. Baiocchi, T. R. Hayes, and R. S. Freund, *Phys. Rev. A* **35**, 559 (1987).
- ⁴¹M. V. Malyshev and V. M. Donnelly, *J. Appl. Phys.* **87**, 1642 (2000).
- ⁴²J. Y. Choe, N. C. M. Fuller, V. M. Donnelly, and I. P. Herman, *J. Vac. Sci. Technol. A* **18**, 2669 (2000).
- ⁴³*Principles of Plasma Discharges and Materials Processing*, edited by M. A. Lieberman and A. J. Lichtenberg (Wiley, New York, 1994).
- ⁴⁴G. P. Kota, J. W. Coburn, and D. B. Graves, *J. Vac. Sci. Technol. A* **16**, 270 (1998).
- ⁴⁵For 96% Ar plasma, given $T_e = 6.0$ eV and a "tail" temperature of ~ 2.5 eV, the inelastic scattering rate constant for Ar in its ground state is $5 \times 10^{-10} \text{ cm}^3 \text{ s}^{-1}$, due mainly to excitation to the $1s_3$ and $1s_5$, metastable states and to the $2p_x$ ($x = 1-10$) emitting levels (Refs. 46 and 47), while that of the metastable states is $\sim 1 \times 10^{-7} \text{ cm}^3 \text{ s}^{-1}$ (Ref. 48). Using these rate constants, an Ar density of $\sim 3.5 \times 10^{14} \text{ cm}^{-3}$ and a metastable density of $\sim 1 \times 10^{11} \text{ cm}^{-3}$, the electron-neutral collisional frequency, ν_{e-n} is $\sim 10^5 \text{ s}^{-1}$, while the electron-electron collisional frequency (Ref. 49) ν_{e-e} for collisions between fast (>13 eV) and slow (1-3 eV) electrons is $\sim 5 \times 10^3 \text{ s}^{-1}$.
- ⁴⁶The rate constant from the Ar ground state to $1s_3$ and $1s_5$ metastable states is calculated from cross sectional data presented in R. S. Schappe, M. Bruce Shulman, L. W. Anderson, and C. C. Lin, *Phys. Rev. A* **50**, 444 (1994), assuming a Maxwellian EEDF.
- ⁴⁷The rate constant from the Ar ground state to $2p_x$ levels is calculated from cross sectional data presented in J. E. Chilton, J. B. Boffard, R. S. Schappe, and C. C. Lin, *Phys. Rev. A* **57**, 267 (1998), assuming a Maxwellian EEDF.
- ⁴⁸The rate constant from the $1s_3$ and $1s_5$ metastable states to the $2p_x$ levels is calculated from cross sectional data presented in J. B. Boffard, G. Piech, M. Gehrke, L. W. Anderson, and C. C. Lin, *Phys. Rev. A* **59**, 2749 (1999).
- ⁴⁹ ν_{e-e} is calculated from the expression in *Principles of Plasma Discharges and Materials Processing*, edited by M. A. Lieberman and A. J. Lichtenberg (Wiley, New York, 1994), p. 59, determining the density of slow (1-3 eV) electrons assuming a Maxwellian EEDF.